Protective effects of an anti-4-HNE monoclonal antibody against liver injury and lethality of endotoxemia in mice

Handong Qiao[a*], Yuta Morioka[a*], Dengli Wang[a], Keyue Liu[a], Shangze Gao[a], Hidenori Wake[a§], Daiki Ousaka[a], Kiyoshi Teshigawara[a], Shuji Mori[b], Masahiro Nishibori[c]

[a] *Department of Pharmacology, Okayama University Graduate School of Medicine, Dentistry and Pharmaceutical Sciences, Okayama 700-8558, Japan*

[b] *Department of Pharmacology, Shujitsu University, Okayama 703-8516, Japan*

[c] *Department of Translational Research and Drug Development, Okayama University Graduate School of Medicine, Dentistry and Pharmaceutical Sciences. Okayama 700-8558, Japan*

§ Present address: Department of pharmacology, Faculty of Medicine, Kindai University, Osaka-Sayama, 589-8511, Japan

*These authors contributed equally to this work.

Correspondence to: Masahiro Nishibori, MD, PhD.

Department of Translational Research and Drug Development, Okayama University Graduate School of Medicine, Dentistry and Pharmaceutical Sciences, Okayama 700-8558, Japan.

Phone: +81-86-235-7393

Email: mbori@md.okayama-u.ac.jp

ABSTRACT

4-hydroxy-2-nonenal (4-HNE) is a lipid peroxidation product that is known to be elevated during oxidative stress. During systemic inflammation and endotoxemia, plasma levels of 4-HNE are elevated in response to lipopolysaccharide (LPS) stimulation. 4-HNE is a highly reactive molecule due to its generation of both Schiff bases and Michael adducts with proteins, which may result in modulation of inflammatory signaling pathways. In this study, we report the production of a 4-HNE adduct-specific monoclonal antibody (mAb) and the effectiveness of the intravenous injection of this mAb in ameliorating LPS-induced endotoxemia and liver injury in mice. Endotoxic lethality was suppressed by the administration of anti-4-HNE mAb. After LPS injection, we observed a significant increase in the plasma levels of AST, ALT, IL-6, TNF-α and MCP-1, and elevated expressions of IL-6, IL-10 and TNF-α in the liver. All these elevations were inhibited by anti-4-HNE mAb treatment. As to the underlining mechanism, anti-4-HNE mAb inhibited the elevation of plasma high mobility group box-1 (HMGB1) levels, the translocation and release of HMGB1 in the liver and the formation of 4-HNE adducts themselves, suggesting a functional role of extracellular 4-HNE adducts in hypercytokinemia and liver injury associated with HMGB1 mobilization. In summary, this study reveals a novel therapeutic application of anti-4-HNE mAb for endotoxemia.

Keywords: 4-HNE, anti-4-HNE mAb, LPS, endotoxemia, sepsis, acute liver failure

Abbreviations: Anti-4-HNE mAb, anti-4-hydroxy-2-nonenal monoclonal antibody; KLH, keyhole limpet hemocyanin; hr, hour/hours; BSA, bovine serum albumin; rat-SA, rat serum albumin; rabbit-SA, rabbit serum albumin; HSA, human serum albumin; LPS, lipopolysaccharides; AST, aspartate aminotransferase; ALT, alanine aminotransferase; HMGB1, high mobility group box-1; iNOS, inducible nitric oxide synthase; COX-2, cyclooxygenase 2; PBS, phosphate-buffered saline.

1. Introduction

Systemic inflammation is a common symptom of sepsis, and can result in cell death (Andreasen et al., 2008). Endotoxemia is a model of systemic inflammation that can be experimentally elicited in animals by lipopolysaccharide (LPS) administration (Sunil et al., 2007; Andreasen et al., 2008; Ko et al., 2008; Choi et al., 2013; Jiang et al., 2018; Lasselin et al., 2021). LPS causes excessive accumulation of lipid peroxidation products in mice (Mello et al., 2013; Li et al., 2020). 4-hydroxy-2-nonenal (4-HNE) is one of the most frequently studied products of lipid peroxidation from unsaturated fatty acids, and 4-HNE has been shown to form adducts with proteins through Michael addition and Schiff base formation (Andringa et al., 2014; Barrera et al., 2015; Gegotek and Skrzydlewska, 2019).

Earlier studies have repeatedly documented that plasma 4-HNE is a biomarker for lipid peroxidation (Deng et al., 2007; Jackson et al., 2010; Ravera et al., 2015; Podszun et al., 2020). In addition, when produced excessively in cells, 4-HNE may create adducts with proteins, resulting in an antioxidant response, inflammation and apoptosis (Barrera et al., 2015; Gegotek and Skrzydlewska, 2019). When injected intraperitoneally, 4-HNE has been shown to exacerbate colonic inflammation through activation of Toll-like receptor 4 signaling (Wang et al., 2019). A high concentration (40 μM) of 4-HNE induces apoptosis of human retinal pigment epithelial cells by modifying HSP70 (Yang et al., 2019). 4-HNE has also been shown to induce hepatic cytotoxicity by activating the ROS-mediated effects on the JNK MAPK and p38 MAPK pathways (Song et al., 2017). Collectively, these findings suggest a critical role for 4-HNE in the progression of septic conditions.

High mobility group box-1 (HMGB1) is a DNA-binding protein that has distinct

functions depending on its subcellular localization (Zhou et al., 2011; Rao et al., 2017). HMGB1 is mobilized from the nucleus into the cytoplasm/extracellular space during inflammatory responses (Willingham et al., 2009; Lamkanfi et al., 2010; Lu et al., 2012; Lu et al., 2013). Studies using a neutralizing antibody (Ab) against HMGB1 showed that systemic treatment with the Ab conferred protection against brain injuries induced by ischemia, hemorrhage and trauma and improved neurological deficits in rats (Liu et al., 2007; Zhang et al., 2011; Wang et al., 2017). Extracellular HMGB1 appears to disrupt the blood–brain barrier under these insults and to subsequently enhance the brain inflammatory responses through the activation of glial elements (Wang et al., 2017; Nishibori et al., 2020). In addition to brain inflammatory responses, HMGB1 has been shown to be involved in many inflammatory disease conditions (Andersson and Tracey, 2011; Nishibori et al., 2019). In their initial study of HMGB1, Wang et al. (1999) identified and characterized HMGB1 as a late mediator of endotoxic lethality. These findings suggest that LPS-induced endotoxemia might be ameliorated by targeting HMGB1. Additionally, previous studies demonstrated that two inflammatory mediators, i.e., inducible nitric oxide synthase (iNOS) and cyclooxygenase (COX-2), are involved in sepsis (Yu et al., 2017; Natarajan et al., 2018; Singh et al., 2020). Moreover, 4-HNE has been shown to induce iNOS/COX-2 overexpression (Kumagai et al., 2004; Park et al., 2013; Gargiulo et al., 2018).

In the present study, we report the production of a 4-HNE-specific monoclonal antibody (mAb) and evaluate its effectiveness against endotoxemia in mice. We found that the treatment with anti-4-HNE mAb ameliorated the lethality of mice and reduced the liver injury, in association with an inhibition of HMGB1 mobilization, cytokine production and 4-HNE adducts overexpression. Our study strongly suggested that the

extracellular 4-HNE adducts amplify the inflammation in endotoxemia and that anti-4-HNE mAb may provide a novel therapeutic agent for endotoxemia.

2. Materials and methods

2.1. Production of anti-4-HNE mAb

We produced a series of rat monoclonal antibodies (mAbs) that recognize the protein adducts formed by aldehydes derived from sugar metabolism or unsaturated fatty acids in the plasma membrane. Briefly, D-glucose, glyceraldehyde, glycolaldehyde, methylglyoxal, glyoxal, CRA, MDA and 4-HNE were incubated with bovine serum albumin (BSA), rat serum albumin (rat-SA), rabbit serum albumin (rabbit-SA) and human serum albumin (HSA) for 24 hr at 37°C. After extensive dialysis of the incubation mixture against phosphate-buffered saline (PBS), rats were immunized with these protein adducts and iliac lymph node cells were extracted from the immunized rats 2–3 weeks thereafter. The lymph node cells were fused with mouse myeloma cells to produce a hybridoma. We cultured the hybridoma cells and measured their levels of the 4-HNE-specific mAb by ELISA, followed by cloning. Antibody (#13-1-1) was purified with MEP HyperCel resin (Pall Biosepra, Cergy, France) in 50 mM sodium citrate (PH 3.5), followed by PBS dialysis.

2.2. Animals

Adult male C57BL/6N mice (22 ± 3 g, 8 weeks) were purchased from SLC (Hamamatsu, Japan) and then housed in the institutional animal units of Okayama University under a 12-hr light/dark cycle. The mice were maintained on a standard rodent diet with free access to water. Up to four mice were kept per plastic cage with aspen wood bedding material. All experimental procedures were conducted in

accordance with Okayama University guidelines for animal experiments and were approved by the university committee on animal experimentation.

2.3. Endotoxemia model

The endotoxemia model was induced by an intravenous injection of LPS (10 mg/kg). The mice were treated with α-4-HNE mAb (1 mg/kg), α-KLH mAb (1 mg/kg) and PBS 30 min after LPS injection, then sacrificed under deep anesthesia at 16 hr, 20 hr and 24 hr after treatment with the mAbs.

2.4. Murine sepsis score assay

Sickness behaviors were evaluated at 6, 12 and 24 hr. The severity of endotoxemia was assessed using the following indices: appearance, level of consciousness, activity, response to stimulus, eyes, respiration rate, respiration quality. Each of these indices was assigned a score of 1 to 5 as follows: 1 = normal, active; 2 = slightly suppressed activity; 3 = severe illness; 4 = no activity; 5 = death (Shrum et al., 2014; Wake et al., 2016).

2.5. AST/ALT assay

Plasma AST and ALT levels were determined by DRI-CHEM (DRI-CHEM 7000V (Z); Fuji Film, Tokyo, Japan) at the Department of Animal Resources, Advanced Science Research Center, Okayama University, Japan. Briefly, mouse blood was collected into a pre-chilled tube containing EDTA-2K. After centrifugation at 3000 rpm for 10 min, protease inhibitor cocktail (Sigma, St. Louis, MO) was added to the resultant plasma, which was then analyzed to determine the levels of AST and ALT.

2.6. TUNEL staining

TUNEL staining of liver tissue was performed using an MK500 In Situ Apoptosis Detection Kit according to the manufacturer's instructions (Takara Bio, Nagahama, Japan). Briefly, paraffin-embedded mouse liver sections were immersed 3 times in xylene, for 5 min each time, followed by gradient ethanol hydration. The sections were then permeabilized with 15 μg/ml proteinase K for 15 min. Endogenous peroxidases were inactivated with 3% H_2O_2 for 5 min. 50 μl of TdT enzyme in labeling buffer was added to each section and incubated for 60–90 min at 37°C. After washing with PBS 3 times, 70 μl of anti-FITC HRP conjugate was added to each section and incubated for 30 min at 37°C. The sections were then incubated in DAB- H_2O_2 solution for 15 min. The reaction was stopped by dH_2O. Nuclei were stained by Mayer's hematoxylin. Finally, the sections were mounted with Softmount (Wako, Osaka, Japan) and observed using a fluorescence microscope (BZ-X700; Keyence, Tokyo, Japan).

2.7. H & E staining

Briefly, paraffin-embedded liver sections were immersed in lemosol (Wako) 4 times, followed by immersion in tissue dehydration solution (Wako) 4 times. The nuclei were stained by Mayer's Hematoxylin for 5 min. After washing with water, the cytoplasm was stained by Eosin (Wako) for 30 seconds. The sections were then immersed in dehydration solution (Wako) 4 times and washed by lemosol (Wako) 4 times. Finally, the sections were mounted with Softmount (Wako). The samples obtained at 16 hr, 20 hr and 24 hr were observed using a BZ-8000 or BZ-X700 fluorescence microscope (Keyence).

To examine the degree of acute lung injury, we evaluated its five pathological features, including exudates production, hyperemia/congestion, intra-alveolar hemorrhage/debris, cellular infiltration, and cellular hyperplasia on the H&E stained preparations as described previously (Giangola et al., 2013; Hirano et al., 2015). The severity of each pathological features was evaluated by a score indicating 0 as absent/none, 1 as mild, 2 as to show moderate, and finally 3 for severe injury. The total lung injury score was calculated as the sum of these scores (Suppl. Fig. 2).

2.8. Immunostaining assay

Mouse liver paraffin-embedded sections were prepared for immunofluorescence staining. Primary antibodies including α-CD68 (Abcam ab125212, 1:100), α-F4/80 (Abcam ab6640, 1:100), α-HMGB1 (Abcam ab18256, 1:500) and α-4-HNE (Abcam ab48506, 1:50) were used. In order to investigate the relationship between 4-HNE and HMGB1, double immunostaining was also performed. The sections were then incubated with secondary Abs conjugated with Alexa Fluor 488 (Invitrogen, Carlsbad, CA) or Alexa Fluor 555 (Invitrogen). Nuclei were stained with DAPI for 10 min, and the sections were then mounted with antifade mounting medium (Vectashield). The sections were observed using an LSM 780 confocal microscope (Carl Zeiss, Jena, Germany).

2.9. Western blotting

After addition of protease/phosphatase inhibitors, proteins were extracted from the tissue samples using T-PER™ Tissue Protein Extraction Reagent (Thermo Fisher Scientific, Waltham, MA). An equal amount of protein was electrophoresed on a polyacrylamide gel and transferred onto a PVDF membrane (Bio−Rad, Hercules, CA).

The membrane was blocked with 10% skim milk for 1 hr and incubated with primary Abs detecting β-actin (Santa Cruz sc-47778, 1:1000), HMGB1 (Abcam ab18256, 1:1000), iNOS (Abcam ab178945, 1:1000), COX-2 (Abcam ab179800, 1:2000) overnight at 4°C. Secondary HRP-conjugated Abs were then incubated for 1 hr at RT. The signals were visualized by the luminal−based enhanced chemiluminescence HRP substrate method (Thermo Fisher Scientific). An Image Quant LAS4000 system was used for detection, and images were analyzed with ImageJ software (version 1.52a).

2.10. HMGB1 ELISA

The level of HMGB1 in mouse plasma was measured using an HMGB1 ELISA Kit Exp (Shino-test, Tokyo, Japan) according to the manufacturer's instructions. Briefly, mouse blood was collected into EDTA-2K-containing pre-chilled tube. After centrifugation at 3000 rpm for 10 min, protease inhibitor cocktail (Sigma) was added to the resultant plasma. Then the plasma was used for HMGB1 detection with the ELISA Kit.

2.11. RNA isolation and real-time PCR

Fresh mouse liver tissue was stabilized in RNA stabilization solution (RNAlater Solution; Ambion, Austin, TX) overnight at 4°C, and mRNA was extracted using an RNeasy mini kit (Qiagen, Hilden, Germany). cDNA was synthesized with a Takara RNA PCR kit (version 3.0: Takara Bio) according to the manufacturer's instructions. Real−time PCR was performed with a Light Cycler (Roche, Basel, Switzerland) according to the manufacturer's instructions. The primers shown in Table S1 were used to amplify specific cDNA fragments. GAPDH expression was used to normalize cDNA levels. The PCR products were analyzed by a melting curve to ascertain the specificity

of amplification, and the relative fold-change in the gene expression levels in samples was calculated with the Δ–Δ Ct method.

2.12. Cytometric bead array

We measured the mouse plasma cytokines after LPS injection at 24 hr by performing a cytometric bead array assay using a Mouse/Rat Soluble Protein Master Buffer Kit and Cytokine Flex Set (BD Biosciences, San Jose, CA) following the manufacturer's instructions. The protocol of this experiment was almost the same as in our previous study (Gao et al., 2019). Briefly, multiple capture beads for IL-6, TNF-α, MCP-1, and IFN-γ were mixed together. The mixed capture beads were then co-incubated with 50 μl of plasma dilution and detection reagent for 2 hr. Finally, the beads were washed carefully and resuspended. Samples were analyzed using a MACSQuant analyzer (Miltenyi Biotec, Bergisch Gladbach, Germany), and the data were analyzed with FCAP Array software.

2.13. Neutralization of anti-4-HNE mAb

Anti-4-HNE mAb (Abcam ab48506) at a final concentration of 14 μg/ml was incubated with BSA-4-HNE, HSA-4-HNE, RSA-4-HNE at a final concentration of 200 μg/ml or PBS at 4°C overnight with gentle rotation. After absorbing the antigen, the mixture was then used to perform immunofluorescence staining of 4-HNE. A secondary Ab conjugated with Alexa Fluor 488 (Invitrogen) was used in this experiment. Nuclei were stained with DAPI for 10 min, and then the sections were mounted with antifade mounting medium (Vectashield). The sections were observed using an LSM 780 confocal microscope (Carl Zeiss).

2.14. Statistical analysis

Data are expressed as mean ± standard deviation (SD) and analyzed using GraphPad Software Prism 7.0. Statistical significance was determined by one-way analysis of variance (ANOVA) followed by Tukey's test or Dunnett's test. The details of each experiment, including the number of samples, are included in the figures' legends. The date analysis of the results of COX-2 expression by Western blot was performed by Mann-Whitney U-test. Differences in values were considered significant if $P < 0.05$.

3. Results

3.1. Characterization and selection of a rat mAb against 4-HNE adducts

Figure 1A shows the protocol for the production of anti-4-HNE-specific mAb. We made an antigen molecule for immunization, i.e., a 4-HNE adduct on rat serum albumin, and immunized rats with this antigen. After obtaining the iliac lymph nodes, we produced a hybridoma by the fusion of rat lymphocytes with mouse myeloma cells as described previously (Liu et al., 2007). We screened the mAbs by means of an ELISA using microtiter plates coated with various albumin adducts, as shown in Fig. 1B. Among the positive clones recognizing 4-HNE-rat SA, a single clone (#13-1-1) did not cross-react with any of the aldehyde adducts on BSA, rat-SA, or HSA, except for 4-HNE adducts on BSA, rabbit-SA and HSA (Fig. 1B). To further evaluate the lab-made anti-4-HNE adduct mAb (#13-1-1), Western blotting was carried out to confirm its specificity. Among the 4-HNE-serum albumins from different species, the mAb (#13-1-1) showed the highest binding to 4-HNE-rat-serum albumin, and it did not show any reaction with cognate rat-serum albumin (Fig. 1C). These results from Western blotting (Fig. 1C) were consistent with those from ELISA (Fig. 1B), except for the weak recognition of 4-HNE-BSA by the mAb on Western blotting. Taken together, the results indicate that we successfully produced a mAb that highly recognizes a 4-HNE-specific adduct on serum albumin.

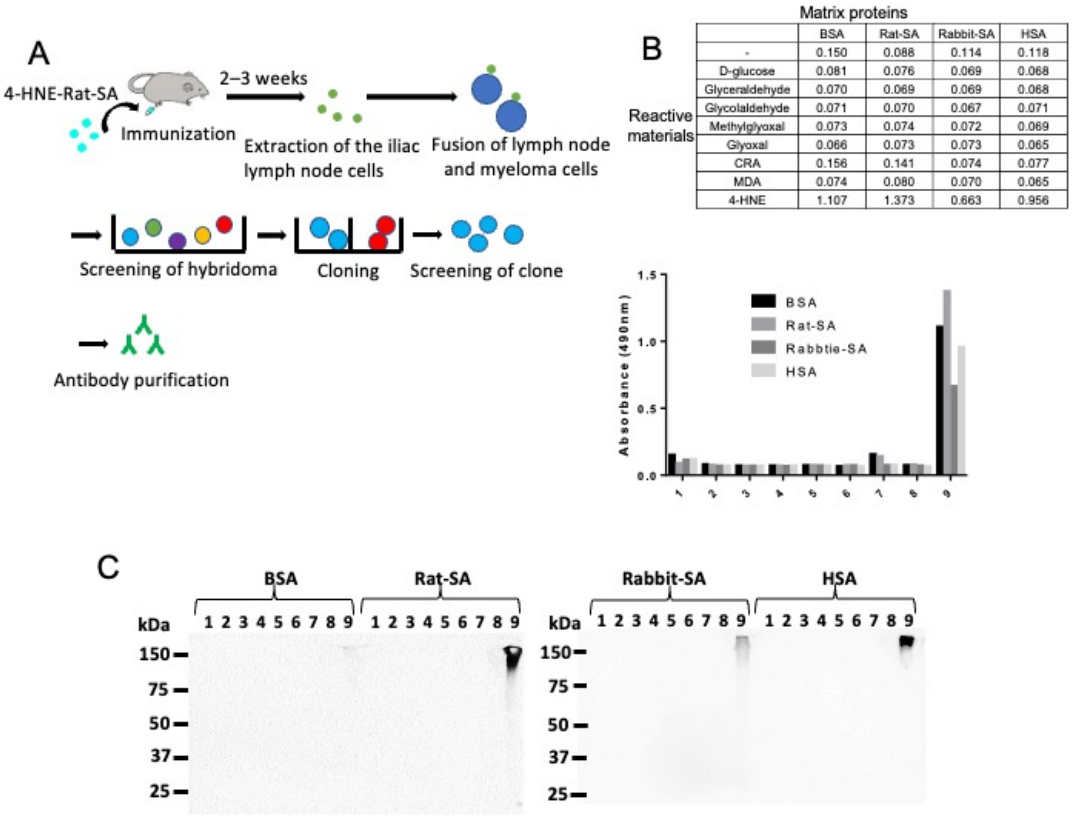

	BSA	Rat-SA	Rabbit-SA	HSA
-	0.150	0.088	0.114	0.118
D-glucose	0.081	0.076	0.069	0.068
Glyceraldehyde	0.070	0.069	0.069	0.068
Glycolaldehyde	0.071	0.070	0.067	0.071
Methylglyoxal	0.073	0.074	0.072	0.069
Glyoxal	0.066	0.073	0.073	0.065
CRA	0.156	0.141	0.074	0.077
MDA	0.074	0.080	0.070	0.065
4-HNE	1.107	1.373	0.663	0.956

Figure 1. Characterization and selection of a rat mAb against 4-HNE adducts. (**A**) Monoclonal Abs were produced as described in the 4-HNE mAb production protocols. (**B**) Advanced lipid peroxidation end products (ALE)-subspecies of D-glucose, glyceraldehyde, glycolaldehyde, methylglyoxal, glyoxal, CRA, MDA and 4-HNE were immobilized at 2 μg/ml, and the mAbs concentration was 1 μg/ml by an ELISA assay. (**C**) Western blotting of 4-HNE-specific monoclonal antibodies. Electrophoresis samples from 1–9 were 1: control albumin; 2: Glc-AGEs, 3: Glycer-AGEs; 4: Glycol-AGEs; 5: MGO-AGEs; 6: GO-AGEs-Rat-SA; 7: CRA; 8: MDA; and 9: 4-HNE.

3.2. Effects of anti-4-HNE mAb treatment on lethality and tissue injuries in endotoxemic mice

Figure 2A shows the protocol used to induce endotoxemia in mice. The administration of anti-4-HNE mAb, anti-KLH mAb or PBS was carried out 30 min after the injection of LPS. The survival rates of endotoxemic mice treated with PBS or anti-KLH control mAb were 30% and 25%, respectively, 6 days after LPS injection (Fig.

2B). Treatment with anti-4-HNE mAb significantly improved the survival rate to 73% (Fig. 2B). We also determined the murine sepsis score (MSS) (Shrum et al., 2014; Wake et al., 2016) within 24 h after LPS injection (Fig. 2C). Mice in the anti-4-HNE mAb-treated group had lower scores compared with those in the PBS- and anti-KLH mAb-treated groups at 24hr after LPS, implying that the general condition of the former mice was improved.

It is well known that multi-organ failure is often observed in lethal endotoxemia. To evaluate the endotoxemia-related tissue injuries and the protective effects of anti-4-HNE mAb, we carried out histological examinations and measured plasma cytokine levels and inflammatory responses in the tissues, with a particular focus on liver and lung injuries.

To evaluate liver injury, we measured the plasma aspartate aminotransferase (AST) and alanine aminotransferase (ALT) levels (Fig. 2D, E). Both plasma AST and ALT were increased after LPS injection. The administration of anti-4-HNE mAb significantly inhibited the increase in AST and ALT, while the control mAb did not produce any effects (Fig. 2D, E). Hematoxylin-eosin (H&E) staining of the liver revealed that LPS induced much larger intercellular gap areas in the PBS- and anti-KLH mAb- treated groups at 24 hr compared with those of the sham and anti-4-HNE mAb-treated groups (Fig. 2F). This was also true for H&E staining at 16 hr and 20 hr (Suppl. Fig. 1A, B). TUNEL staining showed that there were many TUNEL-positive apoptotic cells in the LPS- and anti-KLH mAb-treated groups, but we found a significantly lower number of apoptotic cells by the administration of anti-4-HNE mAb (Fig. 2G).

Supplementary Figure 2 shows the HE-staining of lung tissue with lower and higher

magnifications 20 hr after the injection of LPS. In the control animals treated with PBS or anti-KLH mAb, multiple features of lung inflammatory responses were apparent, including exudate, increased thickness of alveolar walls, leukocyte adhesion/infiltration and congestion. Histological scoring of the lung injury based on the inflammatory responses (Suppl. Fig. 2B) clearly revealed that the lung injury was accompanied by endotoxemia under the present conditions. The effects of the treatment with anti-4-HNE mAb on lung injury were marginal and did not reach the level of statistical significance.

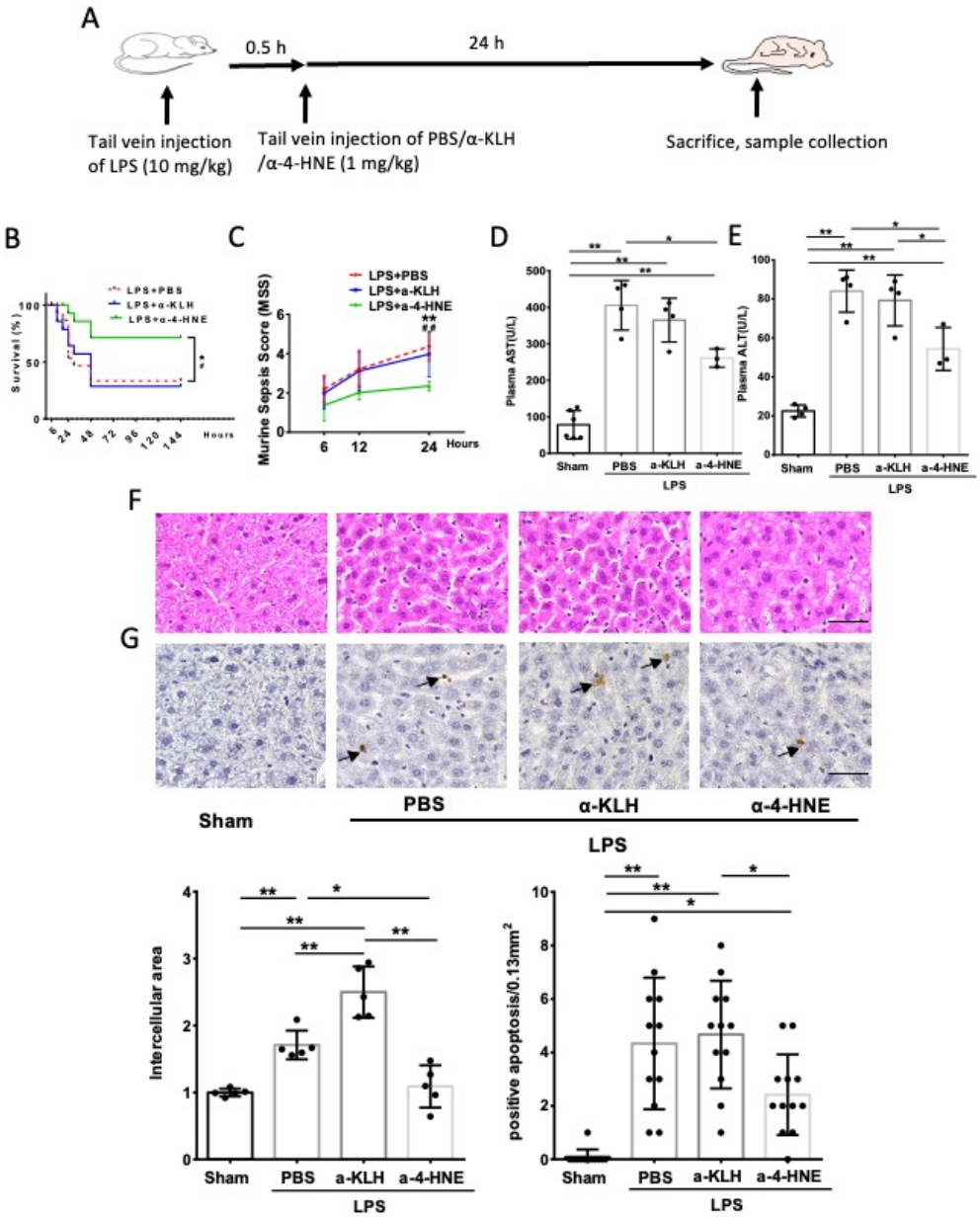

Figure 2. α-4-HNE mAb alleviated LPS-induced endotoxemia in mice. (**A**) The LPS-induced endotoxemia model was established with an intravenous injection of LPS (10 mg/kg), followed by α-KLH/α-4-HNE (1 mg/kg) treatment 30 min thereafter. Mice were sacrificed at 24 h after mAb treatment. (**B**) The survival rate was determined in the LPS+PBS (n=16), LPS+α-KLH (n=15) and LPS+α-4-HNE (n=17) groups. *P<0.05 and #P<0.05 compared with LPS+α-4-HNE group. (**C**) The Murine Sepsis Score (MSS) was measured up to 24 h to assess the severity of endotoxemia in LPS+PBS (n=3), LPS+α-KLH (n=3) and LPS+α-4-HNE (n=3) mice. **P<0.01 and ##P<0.01 compared with LPS+α-4-HNE group. (**D** and **E**) Plasma AST and ALT levels (IU/L) were determined at 24 h. (**F**) Representative H&E staining of liver tissue sections at 24 h are shown. The intercellular areas were determined by ImageJ on each group after mAb treatment. (**G**) Representative TUNEL stainings of liver tissue sections are shown. Arrows indicate TUNEL-positive cells. The results are the means±SD. *P<0.05, **P<0.01, #P<0.05, ##P<0.01. Scale bar = 50 μm.

3.3. Effects of anti-4-HNE mAb treatment on the mRNA expression of inflammation-

related cytokines in the liver and their plasma levels

We found that the expressions of several inflammation-related cytokines, such as IL-6, IL-10 and TNF-α, were markedly induced by LPS at 24 hr, and that these expressions were strongly suppressed by treatment with anti-4-HNE mAb (Fig. 3A). Similar results were observed at both 16 hr and 20 hr after mAb treatment (Suppl. Fig. 3A, B). Moreover, the administration of LPS resulted in a remarkable increase of IL-6, TNF-α, MCP-1 and IFN-γ in the plasma of mice at 24 hr, and these increases were also suppressed by anti-4-HNE mAb treatment (Fig. 3B). The results thus indicated that anti-4-HNE mAb treatment prevented the proinflammatory cytokine responses and suppressed the resultant plasma levels of inflammatory cytokines.

Measurement of the expression of proinflammatory cytokines and other inflammation-related molecules in the lung showed that endotoxemia induced significant increases in the expressions of IL-1β, TNF-α, IL-6, IL-10, MCP-1 and iNOS at 20 hr after LPS (Suppl. Fig. 3). However, among the inflammation-related molecules examined, only the expression of IL-1β was significantly suppressed by the administration of anti-4-HNE (Suppl. Fig. 4).

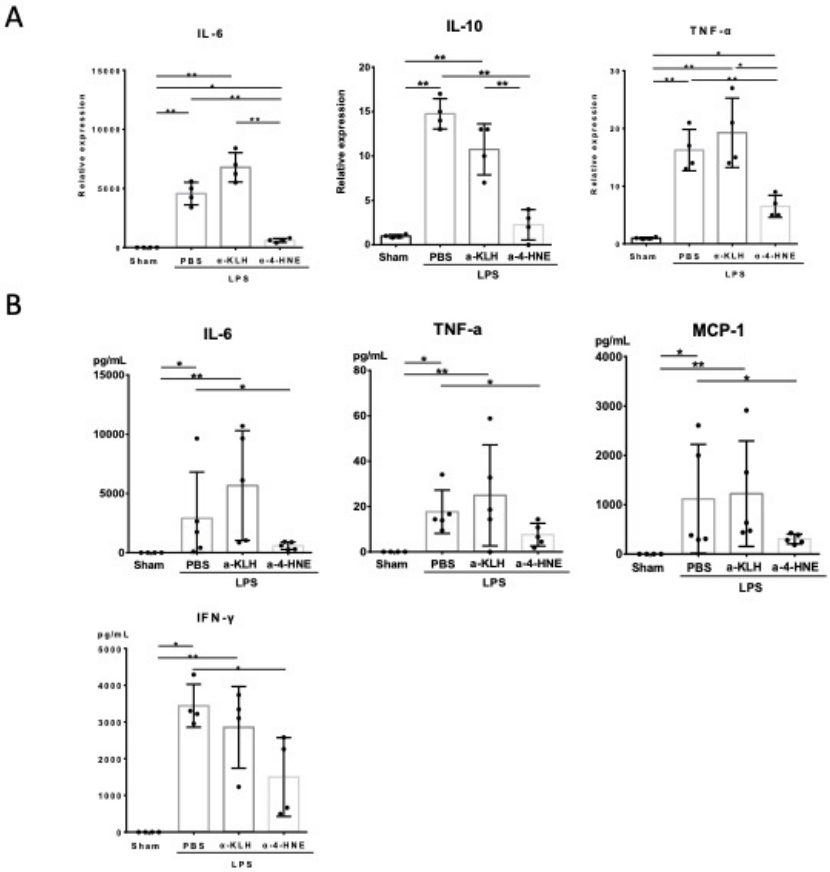

Figure 3. α-4-HNE mAb suppressed mRNA expression and inflammation-related molecules in mouse liver and plasma. Liver and plasma samples were collected 24 h after mAb treatment. (**A**) The mRNA levels of IL-6, IL-10, and TNF-α in the liver were determined by RT-PCR. The results are shown for each group (n=4). (B) The plasma concentrations of IL-6, TNF-α, MCP-1 and IFN-γ were determined by using a Mouse Soluble Protein Master Buffer Kit. The results are shown for each group (n=4). Data are the means±SD. *P<0.05, **P<0.01. One-way ANOVA followed by Tukey's HSD test.

3.4. Anti-4-HNE mAb modulates macrophages and HMGB1 release in liver

To investigate the mechanism underlying the protective effects of anti-4-HNE mAb on the endotoxemic mouse liver, we examined the distribution of macrophages in the liver tissue and the translocation of HMGB1, a representative DAMP, in hepatocytes. There were a considerable number of CD68-positive cells in the livers of sham mice.

Although the administration of LPS did not produce any significant change in the number of CD68-positive cells in PBS-treated or anti-KHL mAb-treated mice, the treatment with anti-4-HNE mAb significantly decreased the number of CD68-positive cells when compared with other LPS-injected groups (Fig. 4A,D). Similarly, we observed a significantly smaller number of F4/80-positive cells in the anti-4-HNE mAb-treated group compared with the PBS and anti-KLH mAb treatment groups in endotoxemic mice (Fig. 4B, D). Next, we stained the liver tissue sections with anti-HMGB1 Ab (Fig. 4C). In sham control mice, HMGB1 was restrictively localized to the nuclei of hepatocytes. Administration of LPS induced a clear translocation of HMGB1 from nuclei to cytosol at 24 hr, while this translocation was significantly suppressed in the anti-4-HNE mAb-treated group (Fig. 4C, D).

To further confirm the effects of anti-4-HNE mAb on HMGB1 translocation and release in the liver, we performed Western blotting of HMGB1 in the liver tissue and determined the plasma HMGB1 levels using ELISA (Fig. 4D, E). The results showed that the liver tissue levels of HMGB1 were decreased after LPS, whereas the plasma levels of HMGB1 were increased 2.5-fold by LPS administration in the PBS- and anti-KLH mAb-treated groups (Fig. 4F). The treatment with anti-4-HNE mAb significantly inhibited the elevation of plasma HMGB1 levels. These results suggested that LPS administration induced the translocation/release of HMGB1 from the liver and other tissues into circulation, and this effect was prevented by anti-4-HNE mAb (Fig. 4D, E).

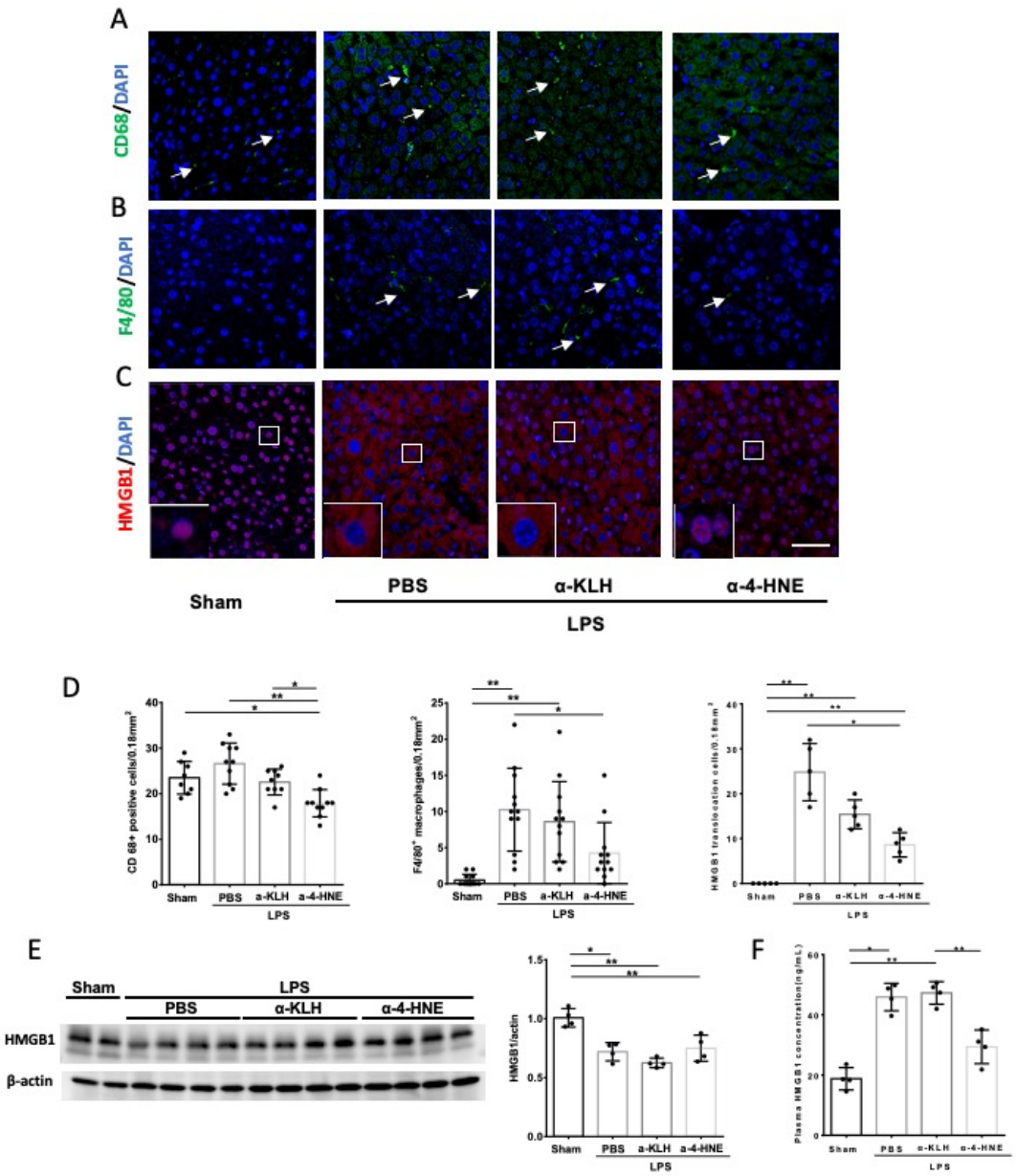

Figure 4. α-4-HNE mAb modulated macrophage and HMGB1 release in the mouse liver. Liver and plasma samples were collected 24 h after mAb treatment. (**A**) The liver sections were stained with α-CD68 Ab. CD68-positive cells are indicated by white arrows. The number of CD68-positive cells in each group was counted. The representative pictures from 4 mice are shown. (**B**) The liver sections were stained with α-F4/80 Ab. F4/80-positive cells are indicated by white arrows. The number of F4/80-positive cells in each group was counted. The representative pictures from 4 mice are shown. (**C**) The liver sections were stained with α-HMGB1 Ab. Cells with HMGB1 translocation were counted. Representative pictures from 4 mice are shown. (**D**) Quantitative analyses of histochemistry. (**E**) The liver HMGB1 level was determined by Western blotting and the quantitative results were calculated using β-actin as a reference (n=4). (**F**) Plasma HMGB1 levels (ng/mL) were measured by ELISA (n=4). Data are the means±SD. *P<0.05, **P<0.01. One-way ANOVA followed by Tukey's HSD test. Scale bars = 50 μm.

3.5. Anti-4-HNE mAb suppresses 4-HNE adducts by modulating HMGB1 release from

the liver

HMGB1/4-HNE double staining suggested that the formation of 4-HNE adducts in the liver tissue may have relevance to the HMGB1 translocation and vice versa at 24 hr (Fig. 5A). Consistent with this result, when we stained liver tissue at 16 hr and 20 hr after mAb treatment, the LPS-induced increase in HMGB1 translocation and 4-HNE adducts formation were reversed by anti-4-HNE mAb treatment (Suppl. Fig. 5A, B). Moreover, we observed a relationship between HMGB1 and the 4-HNE adducts—namely, the activation of HMGB1 translocation/release was inversely correlated with the expression of 4-HNE adducts (Fig. 5B). To check the specificity/accuracy of 4-HNE staining, we neutralized the primary Ab with BSA-4-HNE, HSA-4-HNE and RSA-4-HNE overnight, and found that the nuclear 4-HNE staining vanished, indicating that the reaction was specific for 4-HNE adducts and the major portion of the 4-HNE adducts may have been located in the hepatocyte nuclei (Suppl. Fig. 6B-E).

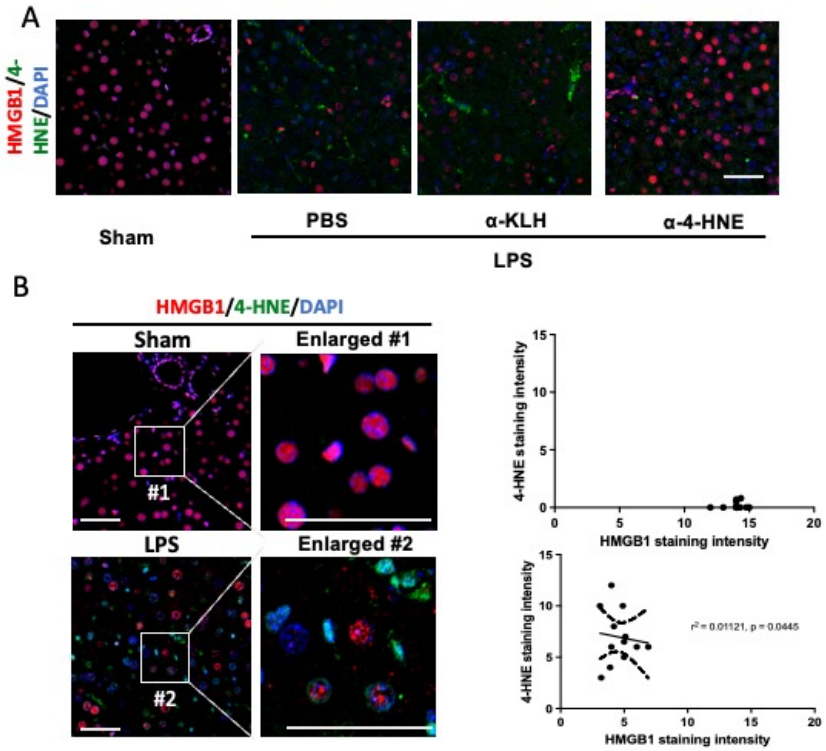

Figure 5. HMGB1 translocation and release were positively correlated with 4-HNE adducts expression. Liver and plasma samples were collected 24 h after LPS stimulation. (**A**) HMGB1/4-HNE double immunofluorescence staining of liver tissue (n=4). (**B**) 4-HNE and HMGB1 were stained in a Sham group and LPS group. Staining intensity of HMGB1 was plotted as a function of 4-HNE intensity. Linear regression analysis was performed to derive the trend line, r^2 and p value. The dotted curve indicates the 90% confidence interval. Results are plotted for 12 views for each of the two groups. Scale bar = 50 µm.

3.6. Effects of anti-4-HNE mAb on iNOS/COX-2 levels in the liver

To further clarify the protective effects of anti-4-HNE mAb, we examined the expression of two other inflammation-related molecules, iNOS and COX-2 (Fig. 6A). The Western blotting showed that LPS significantly induced both iNOS and COX-2, and treatment with anti-4-HNE mAb suppressed the elevations of iNOS and COX-2 expression (Fig. 6B).

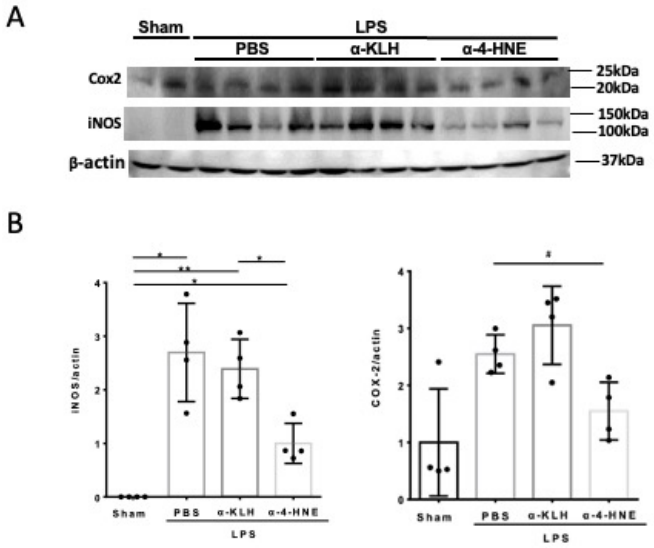

Figure 6. α-4-HNE mAb prevented COX-2/iNOS overexpression in endotoxemic mice. Liver samples were collected 24 h after LPS stimulation. (**A**) COX-2 and iNOS were determined by Western blotting of mouse liver tissue. (**B**) Quantification of Western blotting results. Data are the means±SD of 4 mice. *P<0.05, **P<0.01. One-way ANOVA followed by Tukey's HSD test (left). #P<0.05. The statistical analysis was done using the Mann–Whitney test (right).

4. Discussion

Reactive oxygen species (ROS) are now recognized as very important factors in the process of tissue injury, innate immunity and cell death (Ayala et al., 2014; Schauer et al., 2015). ROS may be produced in response to different exogenous stimuli—such as ionizing radiation, ultraviolet rays, pathogen infections and environmental toxins—that result in an imbalance between the prooxidant and antioxidant levels in favor of prooxidants. Once produced, ROS in turn facilitate the auto-oxidation of unsaturated fatty acids such as arachidonic acid in the cell membrane, leading to the formation and release of reactive aldehydes including 4-HNE, malonedialdehyde and crotonaldehyde (Fritz and Petersen, 2013; Schauer et al., 2015). The released 4-HNE appears to be very active and form adducts with proteins, nucleic acids and lipids (Perluigi et al., 2012; Fritz and Petersen, 2013), resulting in the modulation of transcription, metabolism and cellular signaling (Ayala et al., 2014; Schauer et al., 2015). There are many reports showing marked increases in the plasma protein adducts of 4-HNE under different disease conditions involving tissue injuries and oxidative stress (Ayala et al., 2014; Schauer et al., 2015). Therefore, plasma 4-HNE adducts have been used as effective biomarkers of oxidative stress in the affected tissues (Schauer et al., 2015). However, few studies have examined the causal relationship between the existence of extracellular 4-HNE adducts and the enhancement of the inflammatory responses that lead to tissue damage, such as cytokine/chemokine production, vascular hyperpermeability, and leukocyte infiltration.

In the present study, to evaluate the possible involvement of extracellular 4-HNE adducts in tissue injury and inflammation, we produced a mAb specific for a 4-HNE-adduct. Namely, mAb #13-1-1 recognized a 4-HNE-specific adduct of rat serum

albumin, which cross-reacted with the 4-HNE adducts of various serum albumins from different animals (Fig. 1). In addition, this anti-4HNE mAb did not recognize 8 other aldehyde-derived adducts (Fig. 1). These results indicated that, among the structurally relevant adducts, the anti-4-HNE mAb (#13-1-1) was specific for a 4-HNE adduct and recognized a similar epitope on protein substrates beyond species (Campos-Pinto et al., 2019). When administered intravenously to mice, the anti-4-HNE mAb probably first encounters the antigen in the plasma or extracellular space. In our experiments, neutralization and/or removal of 4-HNE adducts by the specific anti-4-HNE mAb improved the survival of endotoxemic mice (Fig. 2B). As to the underlying mechanism, the anti-4-HNE mAb appeared to exert beneficial effects on liver inflammation by inhibiting cytokine production (Fig. 3), HMGB1 mobilization and macrophage activation (Fig. 4).

LPS is a representative PAMP of bacterial origin, and one of the ways it reaches the liver is via translocation from the gut (i.e., pathological bacterial translocation). The translocation of a small amount of LPS from the gut to the liver is now recognized as a cause of metabolic endotoxemia (Fuke et al., 2019; Mohammad and Thiemermann, 2020), which may orchestrate the intercellular response in the liver micromilieu and regulate the metabolic balance through the detection of LPS (Ferro et al., 2020; Mohammad and Thiemermann, 2020). Thus, the liver appears to play a major role in the response to LPS as well as in the detection and clearance of LPS from the bloodstream. In addition, relatively high levels of LPS are known to induce systemic endotoxemia with hypercytokinemia, endothelial disorder, and microcirculatory failure, which has been repeatedly used for evaluating the systemic inflammation in animals (Bannerman and Goldblum, 2003; Dickson and Lehmann, 2019). LPS is first

recognized by pattern recognition receptors that trigger an innate immune response. The involvement of toll-like receptor-4 (TLR4)/MD2/CD14 in the recognition of LPS molecules on the macrophage cell surface has been well established (Takeda and Akira, 2004;Yamamoto et al., 2004). After the engagement of LPS with the receptor complex, the MyD88, TIRAP and IRAK activation cascade leads to the activation of NF-kB or MAP kinases, resulting in the inflammatory responses. RAGE may be another pattern-recognition receptor which triggers the NF-kB pathway in macrophages (Yamamoto et al., 2011). Recent studies have also demonstrated that LPS may be incorporated into hepatocytes and induce the production of cytokines such as IL-1β and IL-18 through caspase-dependent and gasdermin D-dependent processes (Deng et al., 2018; Li et al., 2020a). During the process of LPS uptake into hepatocytes, HMGB1 may play a carrier-like role by complex formation with LPS and subsequent incorporation into hepatocytes via endocytotic process (Deng et al., 2018; Li et al., 2020a). Thus, HMGB1 translocation and release from the hepatocytes observed under endotoxemia appear to be intimately linked to LPS stimulation and uptake (Deng et al., 2018; Li et al., 2020a), leading to efficient amplification of the responses to LPS through the production of proinflammatory cytokines. During these processes, it is quite likely that the production of 4-HNE occurs in the liver tissue, and indeed, hepatic localization of 4-HNE was histochemically confirmed in our experiments (Fig. 5 and Suppl. Fig. 5). In addition, the production of 4-HNE adducts in the liver in endotoxemic rats/mice has been reported by other groups (Zhang et al., 2000; Gujral et al., 2004; Sakaguchi and Fujisawa, 2006). In the present study, we found that the mRNA expression of cytokines such as IL-6 and TNF-α was induced in the liver of endotoxemic mice, and this expression was strongly inhibited by the administration of the anti-4HNE mAb. Anti-

4-HNE mAb also inhibited the translocation of HMGB1 in and release of HMGB1 from hepatocytes. Consequently, it is apparent that LPS-induced responses such as HMGB1 release, cytokine production and 4-HNE formation (Figs. 3, 4, and 5) were interrelated in the liver and that the 4-HNE adducts in the extracellular space may amplify the responses to LPS while linking each event. Such a relationship might be a reason why the treatment with anti-4HNE mAb efficiently suppressed the LPS-induced liver injury with the elevation of AST and ALT in plasma, leading to the improvement of lethality of endotoxic mice. In our previous studies (Zhang et al., 2011; Wang et al., 2022a), we observed that the administration of neutralizing mAb against HMGB1 to rats with brain ischemia/reperfusion or hemorrhage not only suppressed the mobilization and release of HMGB1 in the brain but also inhibited the production of 4-HNE adducts in plasma and in the brain tissue. These results also support the idea that the actions of HMGB1 and the production of 4-HNE adducts are closely related, and are consistent with the present results mentioned above.

Previous studies indicated that macrophages are involved in LPS-induced hepatic damage (Song et al., 2003; Pervin et al., 2018; Schippers et al., 2020). It has also been conjectured that LPS may alter the liver microenvironment by modulating M1 and M2 macrophage-related inflammatory mediators and macrophage-based hepatotoxicity (Rankine et al., 2006; Pervin et al., 2018). Consistent with this idea, when we stained macrophages in liver tissue with CD68 and F4/80, positivity for both markers was increased after LPS challenge, but neither CD68 nor F4/80 positivity was significantly increased in the anti-4-HNE mAb treatment group. Our results on CD68 and F4/80 staining suggest that anti-4-HNE mAb administration prohibited the macrophage activation. The upregulation of iNOS /COX-2 in the liver observed in the present study

was consistent with the findings reported previously in septic animals (Natarajan et al., 2018; Singh et al., 2020). This upregulation was inhibited by anti-4-HNE mAb. Compared with the effects on liver injury, the effects of anti-4HNE mAb on lung injury were marginal (Suppl. Fig. 2 and Suppl. Fig. 6), suggesting that extracellular 4-HNE adducts made only a minor contribution to the lung injury and inflammation.

Wang et al. (Science, 1999) first reported that HMGB1 may be a late mediator of endotoxemia induced by LPS. HMGB1 appears to have many mechanisms for amplifying systemic inflammation. For example, HMGB1 stimulates plural receptors directly (RAGE and TLR-4/2) and indirectly (CXCR4 and IL-1βR) by complex formation with the respective cytokines, and facilitates the incorporation of pathogen-derived DNA into host cells in association with the activation of inflammasomes. The decreased levels of plasma HMGB1 by anti-4HNE mAb treatment (Fig. 4F) should contribute to the diminution of plasma levels of cytokines (Fig. 3B).

The translocation of gut-derived LPS into the portal vein may occur due to disruption of the intestinal barrier. The gut–liver axis plays an important role not only in the development of liver disease (An et al., 2022) but also in the dysfunction of distal organs other than the liver through the systemic innate immune response (Assimakopoulos et al., 2022; Wang et al., 2022b). Therefore, the existence of extracellular 4-HNE protein adducts may contribute to the amplification of inflammation in the liver and its subsequent spread to distal organs. Further works will be needed to investigate this possibility.

In conclusion, we demonstrated the beneficial effects of a 4-HNE-specific mAb on endotoxemia in mice. The neutralization of 4-HNE adducts present in the extracellular space was shown to lead to a reduction of inflammatory responses in the

liver as well as to reductions in hypercytokinemia and plasma HMGB1. Therefore, plasma 4-HNE adducts are not only biomarkers of systemic oxidative stress but also a possible target for the treatment of endotoxemia and other inflammatory diseases.

Author contributions

Handong Qiao, Yuta Morioka, and Masahiro Nishibori conceived of the project and designed the study. Yuta Morioka, Keyue Liu, and Shuji Mori produced the anti-4-HNE monoclonal antibody and purified it for experiments. Handong Qiao, Dengli Wang, Shangze Gao, and Hidenori Wake were responsible for the acquisition of data. Handong Qiao, Yuta Morioka, Daiki Ousaka, and Kiyoshi Teshigawara performed the data analysis and interpretation. Handong Qiao, Keyue Liu and Masahiro Nishibori wrote the manuscript.

Conflicts of Interest

None of the authors has any conflict of interest to report.

Acknowledgements

This study was supported in part by a JSPS KAKENHI Grant (no. 19H03408) and a grant from the Japan Agency for Medical Research and Development (AMED) (no. 19lm0203008).

References

An, L., Wirth, U., Koch, D., Schirren, M., Drefs, M., Koliogiannis, D., Niess, H., Andrassy, J., Guba, M., Bazhin, A.V., Werner, J., Kuhn, F., 2022. The role of gut-derived lipopolysaccharides and the intestinal barrier in fatty liver diseases. J Gastrointest Surg 26, 671-683.

Andersson, U., Tracey, K.J., 2011. HMGB1 is a therapeutic target for sterile inflammation and infection. Annu Rev Immunol 29, 139-162.

Andreasen, A.S., Krabbe, K.S., Krogh-Madsen, R., Taudorf, S., Pedersen, B.K., Moller, K., 2008. Human endotoxemia as a model of systemic inflammation. Curr Med Chem 15, 1697-1705.

Andringa, K.K., Udoh, U.S., Landar, A., Bailey, S.M., 2014. Proteomic analysis of 4-hydroxynonenal (4-HNE) modified proteins in liver mitochondria from chronic ethanol-fed rats. Redox Biol 2, 1038-1047.

Assimakopoulos, S.F., Eleftheriotis, G., Lagadinou, M., Karamouzos, V., Dousdampanis, P., Siakallis, G., Marangos, M., 2022. SARS CoV-2-Induced Viral Sepsis: The Role of gut barrier dysfunction. Microorganisms 10, 1050.

Ayala, A., Munoz, M.F., Arguelles, S., 2014. Lipid peroxidation: production, metabolism, and signaling mechanisms of malondialdehyde and 4-hydroxy-2-nonenal. Oxid Med Cell Longev 2014, 360438.

Bannerman, D.D., Goldblum, S.E., 2003. Mechanisms of bacterial lipopolysaccharide-induced endothelial apoptosis. Am J Physiol Lung Cell Mol Physiol 284, L899-914.

Barrera, G., Pizzimenti, S., Ciamporcero, E.S., Daga, M., Ullio, C., Arcaro, A., Cetrangolo, G.P., Ferretti, C., Dianzani, C., Lepore, A., Gentile, F., 2015. Role of 4-hydroxynonenal-protein adducts in human diseases. Antioxid Redox Signal 22, 1681-1702.

Campos-Pinto, I., Mendez, L., Schouten, J., Wilkins, J., Fedorova, M., Pitt, A.R., Davis, P., Spickett, C.M., 2019. Epitope mapping and characterization of 4-hydroxy-2-nonenal modified-human serum albumin using two different polyclonal antibodies. Free Radic Biol Med 144, 234-244.

Choi, Y.Y., Kim, M.H., Cho, I.H., Kim, J.H., Hong, J., Lee, T.H., Yang, W.M., 2013. Inhibitory effect of Coptis chinensis on inflammation in LPS-induced endotoxemia. J Ethnopharmacol 149, 506-512.

Deng, M., Tang, Y., Li, W., Wang, X., Zhang, R., Zhang, X., Zhao, X., Liu, J., Tang, C., Liu, Z., Huang, Y., Peng, H., Xiao, L., Tang, D., Scott, M.J., Wang, Q., Liu, J., Xiao, X., Watkins, S., Li, J., Yang, H., Wang, H., Chen, F., Tracey, K.J., Billiar, T.R., Lu, B., 2018. The endotoxin delivery protein HMGB1 mediates Caspase-11-dependent lethality in sepsis. Immunity 49, 740-753 e747.

Deng, Y., Thompson, B.M., Gao, X., Hall, E.D., 2007. Temporal relationship of peroxynitrite-induced oxidative damage, calpain-mediated cytoskeletal degradation and neurodegeneration after traumatic brain injury. Exp Neurol 205, 154-165.

Dickson, K., Lehmann, C., 2019. Inflammatory response to different toxins in experimental sepsis

models. Int J Mol Sci 20, 4341.

Ferro, D., Baratta, F., Pastori, D., Cocomello, N., Colantoni, A., Angelico, F., Del Ben, M., 2020. New Insights into the Pathogenesis of Non-Alcoholic Fatty Liver Disease: Gut-Derived Lipopolysaccharides and Oxidative Stress. Nutrients 12, 2762.

Fritz, K.S., Petersen, D.R., 2013. An overview of the chemistry and biology of reactive aldehydes. Free Radic Biol Med 59, 85-91.

Fuke, N., Nagata, N., Suganuma, H., Ota, T., 2019. Regulation of Gut Microbiota and Metabolic Endotoxemia with Dietary Factors. Nutrients 11, 2277.

Gao, S., Wake, H., Gao, Y., Wang, D., Mori, S., Liu, K., Teshigawara, K., Takahashi, H., Nishibori, M., 2019. Histidine-rich glycoprotein ameliorates endothelial barrier dysfunction through regulation of NF-kappaB and MAPK signal pathway. Br J Pharmacol 176, 2808-2824.

Gargiulo, S., Rossin, D., Testa, G., Gamba, P., Staurenghi, E., Biasi, F., Poli, G., Leonarduzzi, G., 2018. Up-regulation of COX-2 and mPGES-1 by 27-hydroxycholesterol and 4-hydroxynonenal: A crucial role in atherosclerotic plaque instability. Free Radic Biol Med 129, 354-363.

Gegotek, A., Skrzydlewska, E., 2019. Biological effect of protein modifications by lipid peroxidation products. Chem Phys Lipids 221, 46-52.

Giangola, M.D., Yang, W.L., Rajayer, S.R., Nicastro, J., Coppa, G.F., Wang, P., 2013. Growth arrest-specific protein 6 attenuates neutrophil migration and acute lung injury in sepsis. Shock 40, 485-491.

Gujral, J.S., Hinson, J.A., Farhood, A., Jaeschke, H., 2004. NADPH oxidase-derived oxidant stress is critical for neutrophil cytotoxicity during endotoxemia. Am J Physiol Gastrointest Liver Physiol 287, G243-252.

Hirano, Y., Aziz, M., Yang, W.L., Wang, Z., Zhou, M., Ochani, M., Khader, A., Wang, P., 2015. Neutralization of osteopontin attenuates neutrophil migration in sepsis-induced acute lung injury. Crit Care 19, 53.

Jackson, A.C., Kammouni, W., Zherebitskaya, E., Fernyhough, P., 2010. Role of oxidative stress in rabies virus infection of adult mouse dorsal root ganglion neurons. J Virol 84, 4697-4705.

Jiang, Z., Meng, Y., Bo, L., Wang, C., Bian, J., Deng, X., 2018. Sophocarpine attenuates LPS-induced liver injury and improves survival of mice through suppressing oxidative stress, inflammation, and apoptosis. Mediators Inflamm 2018, 5871431.

Ko, K., Yang, H., Noureddin, M., Iglesia-Ara, A., Xia, M., Wagner, C., Luka, Z., Mato, J.M., Lu, S.C., 2008. Changes in S-adenosylmethionine and GSH homeostasis during endotoxemia in mice. Lab Invest 88, 1121-1129.

Kumagai, T., Matsukawa, N., Kaneko, Y., Kusumi, Y., Mitsumata, M., Uchida, K., 2004. A lipid peroxidation-derived inflammatory mediator: identification of 4-hydroxy-2-nonenal as a potential inducer of cyclooxygenase-2 in macrophages. J Biol Chem 279, 48389-48396.

Lamkanfi, M., Sarkar, A., Vande Walle, L., Vitari, A.C., Amer, A.O., Wewers, M.D., Tracey, K.J., Kanneganti, T.D., Dixit, V.M., 2010. Inflammasome-dependent release of the alarmin HMGB1

in endotoxemia. J Immunol 185, 4385-4392.

Lasselin, J., Lekander, M., Benson, S., Schedlowski, M., Engler, H., 2021. Sick for science: experimental endotoxemia as a translational tool to develop and test new therapies for inflammation-associated depression. Mol Psychiatry 26, 3672-3683.

Li, W., Deng, M., Loughran, P.A., Yang, M., Lin, M., Yang, C., Gao, W., Jin, S., Li, S., Cai, J., Lu, B., Billiar, T.R., Scott, M.J., 2020a. LPS induces active HMGB1 release from hepatocytes into exosomes through the coordinated activities of TLR4 and Caspase-11/GSDMD signaling. Front Immunol 11, 229.

Li, Z., Zhao, L., Chen, J., Liu, C., Li, S., Hua, M., Qu, D., Shao, Z., Sun, Y., 2020b. Ginsenoside Rk1 alleviates LPS-induced depression-like behavior in mice by promoting BDNF and suppressing the neuroinflammatory response. Biochem Biophys Res Commun 530, 658-664.

Liu, K., Mori, S., Takahashi, H.K., Tomono, Y., Wake, H., Kanke, T., Sato, Y., Hiraga, N., Adachi, N., Yoshino, T., Nishibori, M., 2007. Anti-high mobility group box 1 monoclonal antibody ameliorates brain infarction induced by transient ischemia in rats. FASEB J 21, 3904-3916.

Lu, B., Nakamura, T., Inouye, K., Li, J., Tang, Y., Lundback, P., Valdes-Ferrer, S.I., Olofsson, P.S., Kalb, T., Roth, J., Zou, Y., Erlandsson-Harris, H., Yang, H., Ting, J.P., Wang, H., Andersson, U., Antoine, D.J., Chavan, S.S., Hotamisligil, G.S., Tracey, K.J., 2012. Novel role of PKR in inflammasome activation and HMGB1 release. Nature 488, 670-674.

Lu, B., Wang, H., Andersson, U., Tracey, K.J., 2013. Regulation of HMGB1 release by inflammasomes. Protein Cell 4, 163-167.

Mello, B.S., Monte, A.S., McIntyre, R.S., Soczynska, J.K., Custodio, C.S., Cordeiro, R.C., Chaves, J.H., Vasconcelos, S.M., Nobre, H.V., Jr., Florenco de Sousa, F.C., Hyphantis, T.N., Carvalho, A.F., Macedo, D.S., 2013. Effects of doxycycline on depressive-like behavior in mice after lipopolysaccharide (LPS) administration. J Psychiatr Res 47, 1521-1529.

Mohammad, S., Thiemermann, C., 2020. Role of metabolic endotoxemia in systemic inflammation and potential interventions. Front Immunol 11, 594150.

Natarajan, K., Abraham, P., Kota, R., Isaac, B., 2018. NF-kappaB-iNOS-COX2-TNF alpha inflammatory signaling pathway plays an important role in methotrexate induced small intestinal injury in rats. Food Chem Toxicol 118, 766-783.

Nishibori, M., Mori, S., Takahashi, H.K., 2019. Anti-HMGB1 monoclonal antibody therapy for a wide range of CNS and PNS diseases. J Pharmacol Sci 140, 94-101.

Nishibori, M., Wang, D., Ousaka, D., Wake, H., 2020. High Mobility Group Box-1 and Blood-Brain Barrier Disruption. Cells 9, 2650.

Park, S., Sung, B., Jang, E.J., Kim, D.H., Park, C.H., Choi, Y.J., Ha, Y.M., Kim, M.K., Kim, N.D., Yu, B.P., Chung, H.Y., 2013. Inhibitory action of salicylideneamino-2-thiophenol on NF-kappaB signaling

cascade and cyclooxygenase-2 in HNE-treated endothelial cells. Arch Pharm Res 36, 880-889.

Perluigi, M., Coccia, R., Butterfield, D.A., 2012. 4-Hydroxy-2-nonenal, a reactive product of lipid

peroxidation, and neurodegenerative diseases: a toxic combination illuminated by redox proteomics studies. Antioxid Redox Signal 17, 1590-1609.

Pervin, M., Karim, M.R., Kuramochi, M., Izawa, T., Kuwamura, M., Yamate, J., 2018. macrophage populations and expression of regulatory inflammatory factors in hepatic macrophage-depleted rat livers under lipopolysaccharide (LPS) treatment. Toxicol Pathol 46, 540-552.

Podszun, M.C., Chung, J.Y., Ylaya, K., Kleiner, D.E., Hewitt, S.M., Rotman, Y., 2020. 4-HNE immunohistochemistry and image analysis for detection of lipid peroxidation in human liver samples using Vitamin E treatment in NAFLD as a proof of concept. J Histochem Cytochem 68, 635-643.

Rankine, E.L., Hughes, P.M., Botham, M.S., Perry, V.H., Felton, L.M., 2006. Brain cytokine synthesis induced by an intraparenchymal injection of LPS is reduced in MCP-1-deficient mice prior to leucocyte recruitment. Eur J Neurosci 24, 77-86.

Rao, Z., Zhang, N., Xu, N., Pan, Y., Xiao, M., Wu, J., Zhou, H., Yang, S., Chen, Y., 2017. 1,25-Dihydroxyvitamin D Inhibits LPS-Induced High-Mobility Group Box 1 (HMGB1) Secretion via Targeting the NF-E2-Related Factor 2-Hemeoxygenase-1-HMGB1 Pathway in Macrophages. Front Immunol 8, 1308.

Ravera, S., Bartolucci, M., Cuccarolo, P., Litame, E., Illarcio, M., Calzia, D., Degan, P., Morelli, A., Panfoli, I., 2015. Oxidative stress in myelin sheath: The other face of the extramitochondrial oxidative phosphorylation ability. Free Radic Res 49, 1156-1164.

Sakaguchi, S., Furusawa, S., 2006. Oxidative stress and septic shock: metabolic aspects of oxygen-derived free radicals generated in the liver during endotoxemia. FEMS Immunol Med Microbiol 47, 167-177.

Schaur, R.J.; Siems, W.; Bresgen, N.; Eckl, P.M. 2015. 4-Hydroxy-nonenal—a bioactive lipid peroxidation product. Biomolecules 5, 2247-2337.

Schippers, M., Post, E., Eichhorn, I., Langeland, J., Beljaars, L., Malo, M.S., Hodin, R.A., Millan, J.L., Popov, Y., Schuppan, D., Poelstra, K., 2020. Phosphate groups in the lipid a moiety determine the effects of LPS on hepatic stellate cells: A Role for LPS-dephosphorylating activity in liver fibrosis. Cells 9, 2708.

Shrum, B., Anantha, R.V., Xu, S.X., Donnelly, M., Haeryfar, S.M., McCormick, J.K., Mele, T., 2014. A robust scoring system to evaluate sepsis severity in an animal model. BMC Res Notes 7, 233.

Singh, G., Kaur, J., Kaur, M., Singh, P., Bhatti, R., 2020. Anti-nociceptive and anti-inflammatory effect of imperatorin: evidences for involvement of COX-2, iNOS, NFkappaB and inflammatory cytokines. Int J Neurosci 130, 176-185.

Song, Q., Guo, R., Wei, W., Lv, L., Song, Z., Feng, R., Li, S., Sun, C., 2017. Histidine-alleviated hepatocellular death in response to 4-hydroxynonenal contributes to the protection against high-fat diet-induced liver injury. Journal of Functional Foods 39, 74-83.

Song, Y., Shi, Y., Ao, L.H., Harken, A.H., Meng, X.Z., 2003. TLR4 mediates LPS-induced HO-1 expression in mouse liver: role of TNF-alpha and IL-1beta. World J Gastroenterol 9, 1799-1803.

Sunil, V.R., Patel, K.J., Nilsen-Hamilton, M., Heck, D.E., Laskin, J.D., Laskin, D.L., 2007. Acute endotoxemia is associated with upregulation of lipocalin 24p3/Lcn2 in lung and liver. Exp Mol Pathol 83, 177-187.

Takeda, K., Akira, S., 2004. Microbial recognition by Toll-like receptors. J Dermatol Sci 34, 73-82.

Wake, H., Mori, S., Liu, K., Morioka, Y., Teshigawara, K., Sakaguchi, M., Kuroda, K., Gao, Y., Takahashi, H., Ohtsuka, A., Yoshino, T., Morimatsu, H., Nishibori, M., 2016. Histidine-Rich Glycoprotein Prevents septic lethality through regulation of immunothrombosis and inflammation. EBioMedicine 9, 180-194.

Wang, D., Liu, K., Wake, H., Teshigawara, K., Mori, S., Nishibori, M., 2017. Anti-high mobility group box-1 (HMGB1) antibody inhibits hemorrhage-induced brain injury and improved neurological deficits in rats. Sci Rep 7, 46243.

Wang, D., Ousaka, D., Qiao, H., Wang, Z., Zhao, K., Gao, S., Liu, K., Teshigawara, K., Takada, K., Nishibori, M., 2022a. Treatment of marmoset intracerebral hemorrhage with humanized Anti-HMGB1 mAb. Cells 11, 2970.

Wang, H., Bloom, O., Zhang, M., Vishnubhakat, J.M., Ombrellino, M., Che, J., Frazier, A., Yang, H., Ivanova, S., Borovikova, L., Manogue, K.R., Faist, E., Abraham, E., Andersson, J., Andersson, U., Molina, P.E., Abumrad, N.N., Sama, A., Tracey, K.J., 1999. HMG-1 as a late mediator of endotoxin lethality in mice. Science 285, 248-251.

Wang, H., Zhang, M., Li, J., Liang, J., Yang, M., Xia, G., Ren, Y., Zhou, H., Wu, Q., He, Y., Yin, J., 2022b. Gut microbiota is causally associated with poststroke cognitive impairment through lipopolysaccharide and butyrate. J Neuroinflammation 19, 76.

Wang, Y., Wang, W., Yang, H., Shao, D., Zhao, X., Zhang, G., 2019. Intraperitoneal injection of 4-hydroxynonenal (4-HNE), a lipid peroxidation product, exacerbates colonic inflammation through activation of Toll-like receptor 4 signaling. Free Radic Biol Med 131, 237-242.

Willingham, S.B., Allen, I.C., Bergstralh, D.T., Brickey, W.J., Huang, M.T., Taxman, D.J., Duncan, J.A., Ting, J.P., 2009. NLRP3 (NALP3, Cryopyrin) facilitates in vivo caspase-1 activation, necrosis, and HMGB1 release via inflammasome-dependent and -independent pathways. J Immunol 183, 2008-2015.

Yamamoto, M., Takeda, K., Akira, S., 2004. TIR domain-containing adaptors define the specificity of TLR signaling. Mol Immunol 40, 861-868.

Yamamoto, Y., Harashima, A., Saito, H., Tsuneyama, K., Munesue, S., Motoyoshi, S., Han, D., Watanabe, T., Asano, M., Takasawa, S., Okamoto, H., Shimura, S., Karasawa, T., Yonekura, H., Yamamoto, H., 2011. Septic shock is associated with receptor for advanced glycation end products ligation of LPS. J Immunol 186, 3248-3257.

Yang, L.L., Chen, H., Wang, J., Xia, T., Sun, H., Yuan, C.H., Liu, S.L., Chen, J.B., 2019. 4-HNE induces apoptosis of human retinal pigment epithelial cells by modifying HSP70. Curr Med Sci 39, 442-448.

Yu, L., Yan, J., Sun, Z., 2017. D-limonene exhibits anti-inflammatory and antioxidant properties in

an ulcerative colitis rat model via regulation of iNOS, COX-2, PGE2 and ERK signaling pathways. Mol Med Rep 15, 2339-2346.

Zhang, C., Walker, L.M., Hinson, J.A., Mayeux, P.R., 2000. Oxidant stress in rat liver after lipopolysaccharide administration: effect of inducible nitric-oxide synthase inhibition. J Pharmacol Exp Ther 293, 968-972.

Zhang, J., Takahashi, H.K., Liu, K., Wake, H., Liu, R., Maruo, T., Date, I., Yoshino, T., Ohtsuka, A., Mori, S., Nishibori, M., 2011. Anti-high mobility group box-1 monoclonal antibody protects the blood-brain barrier from ischemia-induced disruption in rats. Stroke 42, 1420-1428.

Zhou, R.R., Zhao, S.S., Zou, M.X., Zhang, P., Zhang, B.X., Dai, X.H., Li, N., Liu, H.B., Wang, H., Fan, X.G., 2011. HMGB1 cytoplasmic translocation in patients with acute liver failure. BMC Gastroenterol 11, 21.

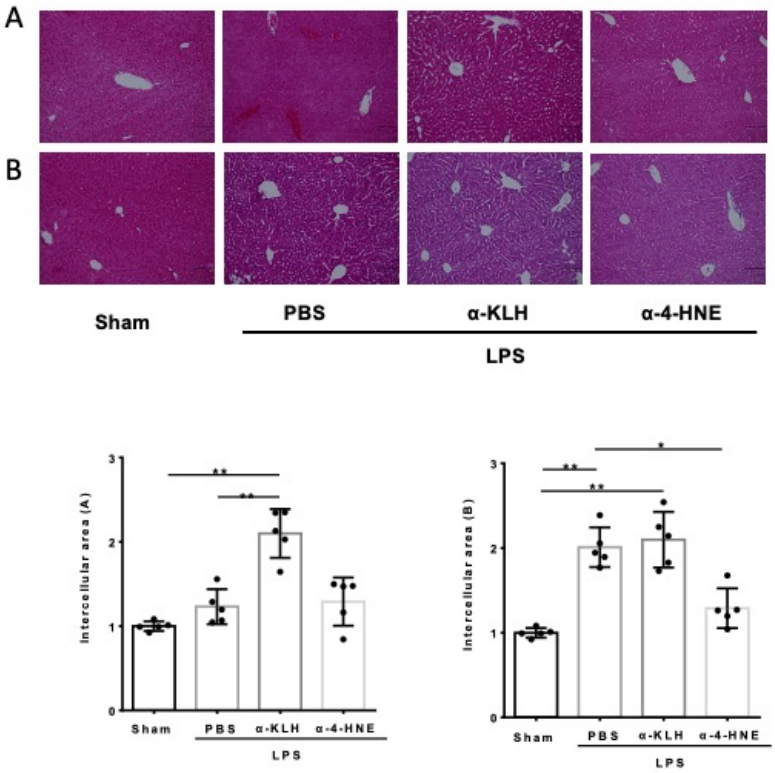

Supplementary Fig. 1. H&E staining of the mouse liver at 16/20 h after mAb treatment. (**A**) Representative H&E staining at 16 h after mAb treatment (n=4). (**B**) Representative H&E staining at 20 h after mAb treatment (n=4). Data are the means±SD. *P<0.05, **P<0.01. One-way ANOVA followed by Tukey's HSD test. Scale bar = 100 μm.

A

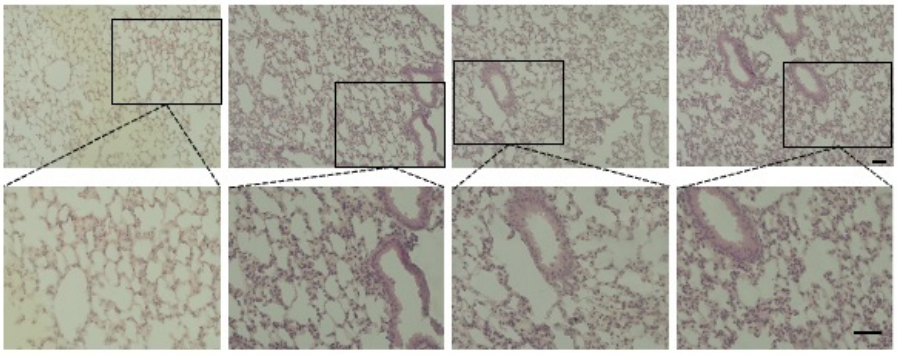

Sham | PBS | α-KLH | α-4-HNE

LPS

B

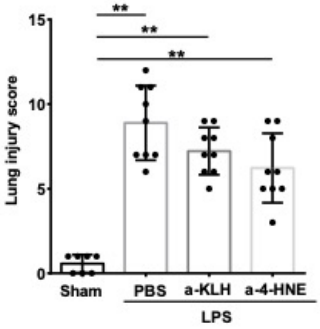

Supplementary Fig. 2. H&E staining of the mouse lung at 20 h after mAb treatment. (**A**) Representative H&E staining at 20 h after mAb treatment (n=3). (**B**) Histological injury scores of the lungs in different groups were quantified as described in the Materials and Methods (n=3). Data are expressed as the means ± SD. **P<0.01. One-way ANOVA followed by Dunnett's test. Scale bar = 50 μm.

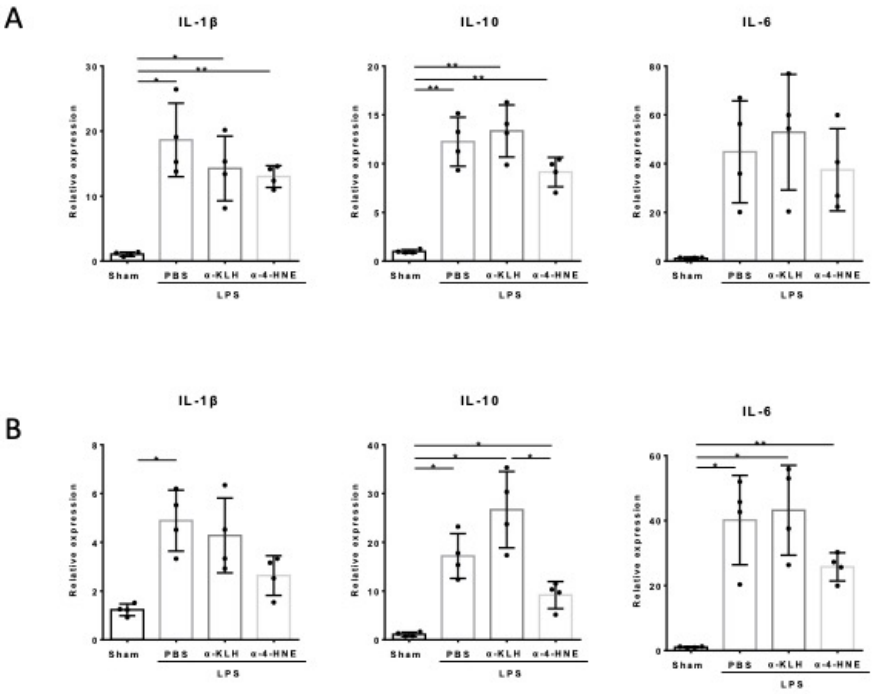

Supplementary Fig. 3. α-4-HNE mAb reduced mRNA expression of inflammation-related molecules in the mouse lung at 16/20 h after mAb treatment. (**A**) The mRNA levels of IL-1β, IL-10 and IL-6 at 16 h are shown from each group (n=4). (**B**) The mRNA levels of IL-1β, IL-10 and IL-6 at 20 h are shown from each group (n=4). Data are the means ±SD. *P<0.05, **P<0.01. One-way ANOVA followed by Tukey´s HSD test.

A

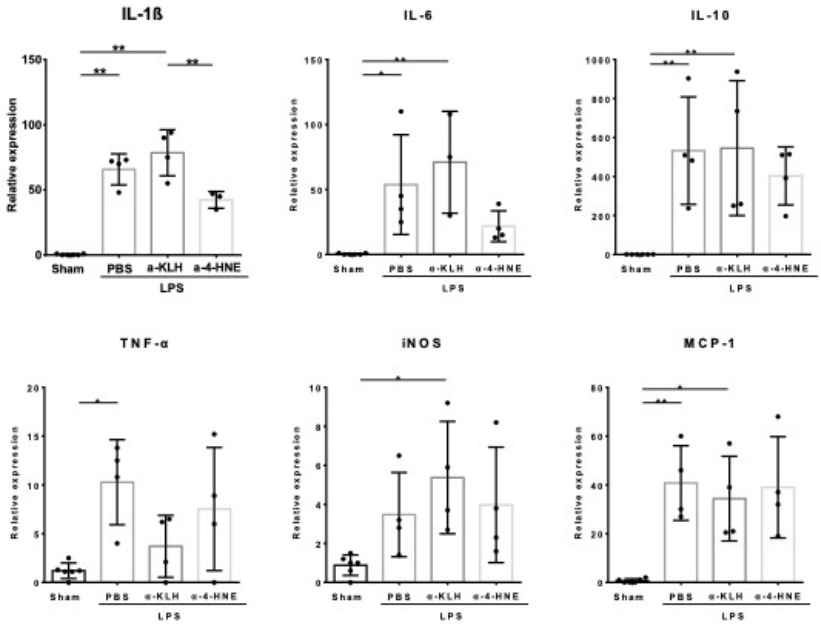

Supplementary Fig. 4. α-4-HNE mAb reduced mRNA expression of inflammation-related molecules in the mouse lung at 20 h after mAb treatment. (**A**) The mRNA levels of IL-1β, IL-6, IL-10, TNF-α, iNOS and MCP-1 at 20 h are shown from each group (n=4). Data are the means ±SD. *P<0.05, **P<0.01. One-way ANOVA followed by Tukey´s HSD test.

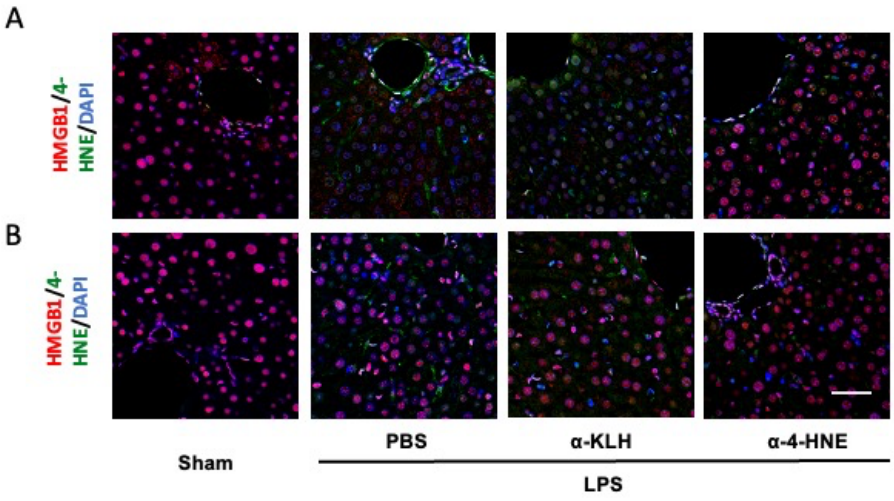

Supplementary Fig. 5. α-4-HNE mAb inhibited HMGB1 translocation and increase of 4-HNE adducts in the mouse liver at 16/20 h after mAb treatment. (**A**) HMGB1/4-HNE double immunofluorescence staining of liver tissue at 16 h after mAb treatment (n=4). (**B**) HMGB1/4-HNE double immunofluorescence staining of liver tissue at 20 h after mAb treatment (n=4). Scale bar=50 μm.

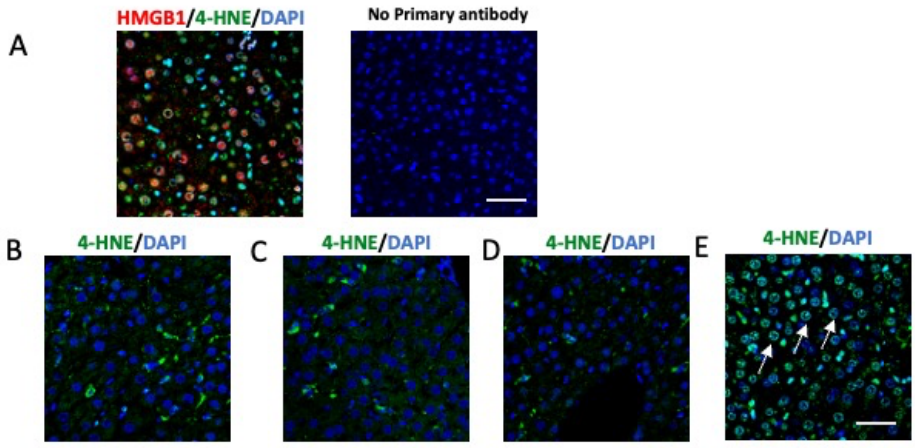

Supplementary Fig. 6. Specificity test for 4-HNE adducts immunofluorescence staining in the mouse liver. (**A**) The left panel shows representative HMGB1/4-HNE double immunofluorescence staining of liver tissue, and the right panel shows liver tissue stained without primary antibody (n=4). (**B**-**D**) Neutralization of 4-HNE primary antibody (ab48506) with BSA-4-HNE, HSA-4-HNE and RSA-4-HNE. (**E**) 4-HNE staining without neutralizer. Scale bar=50 µm.

Supplementary Table S1

Sequences for real-time PCR

Gene	Sequence
GAPDH	Forward 5´-TGACGTGCCGCCTGGAGAAA-3´
	Reverse 5´-AGTGTAGCCCAAGATGCCCTTCAG-3´
IL-6	Forward 5´-GACCTGTCTATACCACTTCACA-3´
	Reverse 5´-CTCTGGAAGTTTCAGATTGTT-3´
IL-10	Forward 5´-ATTTGAATTCCCTGGGTGAGAAG-3´
	Reverse 5´-CACAGGGGAGAAATCGATGACA-3´
IL-1β	Forward 5´-AACCTGCTGGTGTGTGACGTTC-3´
	Reverse 5´-CAGCACGAGGCTTTTTTGTTGT-3´
TNF-α	Forward 5´-GACCCTCACACTCAGATCATCCTTCT-3´
	Reverse 5´-GCGCTGGCTCAGCCACTC-3´
iNOS	Forward 5´-CTGCAGCACTTGGATCAGGAACCTG-3´
	Reverse 5´-GGGAGTAGCCTGTGTGCACCTGGAA-3´
MCP-1	Forward 5´-GCCCCACTCACCTGCTGCTACT-3´
	Reverse 5´-CCTGCTGCTGGTGATCCTCTTGT-3´